Pure Appl. Chem., Vol. 82, No. 4, pp. 1025–1032, 2010.
doi:10.1351/PAC-CON-09-10-04

Radical-substituted dihydrophenazine radical cation salts: Molecular packing structure and bulk magnetic property*

Yuki Masuda, Hirotaka Takeda, Masato Kuratsu, Shuichi Suzuki, Masatoshi Kozaki, Daisuke Shiomi, Kazunobu Sato, Takeji Takui, and Keiji Okada‡

Department of Chemistry, Graduate School of Science, Osaka City University, Sugimoto, Sumiyoshi-ku, Osaka 558-8585, Japan

Abstract: Radical-substituted radical cation salts are exotic species that are potentially applicable as spin building blocks for molecular magnets. We recently found that these species, which are derived from a diphenyldihydrophenazine (**DPP**) framework, are stable under aerated conditions at room temperature. Of these species, nitronyl nitroxide (**NN**$^{\bullet}$)-substituted **DPP**$^{\bullet+}$ tetrachloroferrate (**NNDPP**$^{\bullet\bullet+}$·$FeCl_4^-$) showed antiferromagnetic interaction at low temperature (<150 K), whereas the tetrabromoferrate salt **NNDPP**$^{\bullet\bullet+}$·$FeBr_4^-$ exhibited a magnetic phase transition at 6.7 K to produce a bulk ferrimagnet. Both salts had very similar molecular structures. The difference in the magnetic properties was ascribed to the difference in molecular packing structures. A significant difference in these two salts was observed at the (**NNDPP**$^{\bullet\bullet+}$)–(**NNDPP**$^{\bullet\bullet+}$) intermolecular contact, including the oxygen atom of the nitroxide moiety; **NNDPP**$^{\bullet\bullet+}$·$FeCl_4^-$ had a serious antiferromagnetic O–O (nitroxide oxygen, 3.02 Å) intermolecular contact, whereas **NNDPP**$^{\bullet\bullet+}$·$FeBr_4^-$ had a ferromagnetic O–HC (2.53 Å) intermolecular contact.

Keywords: crystal structure; dihydrophenazine; magnetic properties; nitronyl nitroxide; radical cation.

INTRODUCTION

Radical-substituted radical cations are attractive spin building blocks for organic-based magnets. Yamaguchi and co-workers theoretically explored these species and proposed the possibility of ferro- and ferrimagnets based on radical-substituted charge-transfer (CT) salts [1]. The proposed system involves the following two unique magnetic interactions, J_{intra}: intramolecular magnetic interaction between radical and radical ions, and $J_{interCT}$: intermolecular CT-type magnetic interaction. Although various experimental studies on aniline- [2], ferrocene- [3], and tetrathiafulvalene (TTF)-type donors [2,4,5] with stable radicals have been carried out, the expected magnetic behavior has not been observed. These compounds frequently include a stable radical in a remote position from the radical ion center; this increases chemical stability but decreases the $|J_{intra}|$ value. The difficulty in obtaining the expected properties for these systems may be due to small $|J_{intra}|$ compared to large $|J_{interCT}|$

Pure Appl. Chem.* **82, 757–1063 (2010). An issue of reviews and research papers based on lectures presented at the 13th International Symposium on Novel Aromatic Compounds (ISNA-13), 19–24 July 2009, Luxembourg City, Luxembourg on the theme of aromaticity.
‡Corresponding author

($J_{interCT}$ = –100 to –1000 for typical CT complexes) [6]. Assuming $|J_{interCT}| >> |J_{intra}|$, the system may behave like radical-substituted diamagnetic CT salts showing paramagnetic behavior as has been observed in some cases [2a,5b].

Recently, two types of radical-substituted radical cations showing interesting spintronics behavior have been reported, a diphenyldihydrophenazine (**DPP**)-based system that we reported on previously [7] and benzo-TTF and its selena analogs-based system reported by Sugawara and co-workers [8]. The former exhibits phase transition with $FeBr_4^-$ salt (three-spin system) to a 3D-type ferrimagnet at T_c = 6.7 K, whereas the latter reveals a negative magnetoresistance at low temperature (<20 K). This paper summarizes the development of the radical-substituted **DPP$^{\bullet+}$** system, which constitutes the first experimental demonstration of the Yamaguchi model [1]. As shown later, we prepared two types of nitronyl nitroxide (**NN$^{\bullet}$**)-substituted **DPP$^{\bullet+}$** tetrahaloferrate salts ($FeCl_4^-$ and $FeBr_4^-$) with similar molecular structures. However, the magnetic properties of these salts are very different; the $FeCl_4^-$ salt shows antiferromagnetic interaction without phase transition at low temperature (2–150 K), whereas $FeBr_4^-$ salt shows phase transition at T_c = 6.7 K into a bulk ferrimagnet. The difference is attributed to the molecular packing structures of these salts. These two salts provide textbook examples of how a small difference in molecular packing structures influences the bulk magnetic properties.

EXCHANGE INTERACTION IN NNDPP$^{\bullet\bullet+}$

The 5,10-diphenyl-5,10-dihyrophenazine radical cation (**DPP$^{\bullet+}$**) has large positive spin densities for the nitrogen and C2 carbon atoms [UB3LYP/6-31G(d)]. Therefore, the introduction of **NN$^{\bullet}$** on the C2 carbon atom provides a high-spin system through the spin polarization mechanism (Chart 1). This is exemplified for the diamagnetic anion salt **NNDPP$^{\bullet\bullet+}$**·ClO_4^- [7b]. The χ_pT values in the 150–300 K region are almost 1.0 emu K mol^{-1} and gradually decrease below 50 K. This indicates the presence of a large positive J_{intra} (>300 K) between **NN$^{\bullet}$** and **DPP$^{\bullet+}$**. This large ferromagnetic interaction provides an almost 100 % population for the triplet (S = 1) state (g = 2.004 by EPR) at room temperature. Simulations of the χ_pT-T curve using the spin Hamiltonian [$H = -2J_{intra}(\mathbf{S}_{NN1}\cdot\mathbf{S}_{DPP1} + \mathbf{S}_{NN2}\cdot\mathbf{S}_{DPP2}) - 2J_{inter}\mathbf{S}_{DPP1}\cdot\mathbf{S}_{DPP2}$], which is based on the crystal structure, allows the rough estimation of $J_{intra}/k_B \geq$ +700 K and $J_{inter}/k_B \sim$ –18 K in accordance with the theoretical calculation (J_{intra}/k_B = +987 K). The large J_{intra} value ensures that **NNDPP$^{\bullet\bullet+}$** is a promising species for the Yamaguchi model. The J_{inter} value is strongly dependent on the crystal packing structure and should vary with incorporated magnetic anions.

A similar χ_pT-T behavior was also observed for a different radical source derivative, the 2-(2,4-diphenyl-3-oxoverdazyl) (**Vz$^{\bullet}$**)-substituted **DPP** radical cation **VzDPP$^{\bullet\bullet+}$** [9]. These radical substituted radical cations are characterized by a strongly ferromagnetic intramolecular magnetic interaction between the stable radical and **DPP$^{\bullet+}$** spins.

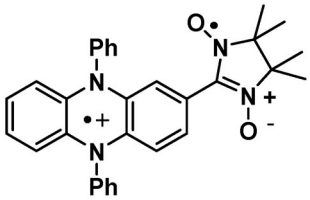

NNDPP$^{\bullet\bullet+}$

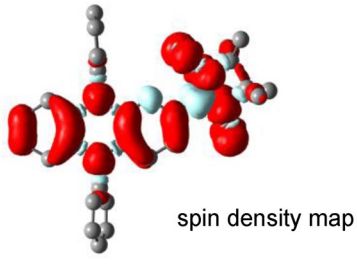

spin density map

Chart 1

NNDPP$^{\bullet+}$·$FeCl_4^-$: ANTIFERROMAGNETIC INTERACTION

Introducing the third spin as a counter anion provides a unique three-spin system. We prepared **NNDPP**$^{\bullet+}$·$FeCl_4^-$ and **NNDPP**$^{\bullet+}$·$FeBr_4^-$ salts ($S_{Fe(III)}$ = 5/2). The former shows antiferromagnetic interaction at low temperature (<150 K), whereas the latter exhibits phase transition at T_c = 6.7 K into a ferrimagnet. The molecular structures of both salts are quite similar. The difference in magnetic behavior is ascribed to the molecular packing structures.

Figure 1 shows the molecular packing structure of **NNDPP**$^{\bullet+}$·$FeCl_4^-$. The crystallographic parameters are summarized in Table 1. The molecular structure of **NNDPP**$^{\bullet+}$ moiety is similar to that of the ClO_4^- salt, although the dihedral angle between the N–C=N plane and the benzo ring attached to the **NN**$^{\bullet}$ group is smaller (7.9º for $FeCl_4^-$ salt, 20.8º for ClO_4^- salt) [7b]. There are several short contacts within or close to the sum of the van der Waals radii between the magnetically important atoms (the Cl atoms in $FeCl_4^-$, C atoms in **DPP**$^{\bullet+}$, and O atoms in **NN**$^{\bullet}$); the intermolecular short contacts are at Cl–C (3.26–3.46 Å), Cl–HC (2.80 Å), O–HC (2.62, 2.68 Å), and O–O (3.02 Å). The C–Cl contacts constitute the column of (–**NNDPP**$^{\bullet+}$–$FeCl_4^-$–**NNDPP**$^{\bullet+}$–$FeCl_4^-$–)$_n$ (in columns I, II, and I*) along the *a*-axis. This is the expected structure in the Yamaguchi model. The C–Cl contact induces antiferromagnetic interaction between **NNDPP**$^{\bullet+}$ (S = 1) and $FeCl_4^-$ (S = 5/2) in accordance with the ferrimagnetic spin alignment. The two O–HC contacts were observed within these columns between **NNDPP**$^{\bullet+}$s. Columns I and II are bound through Cl–HC contacts. Columns II and I* are bridged by O–O contacts. The O–O contact is fatally antiferromagnetic, which may lead to the cancellation of spins of **NNDPP**$^{\bullet+}$s (B and A* in Fig. 1) spins and total magnetizations, and hence no net magnetization.

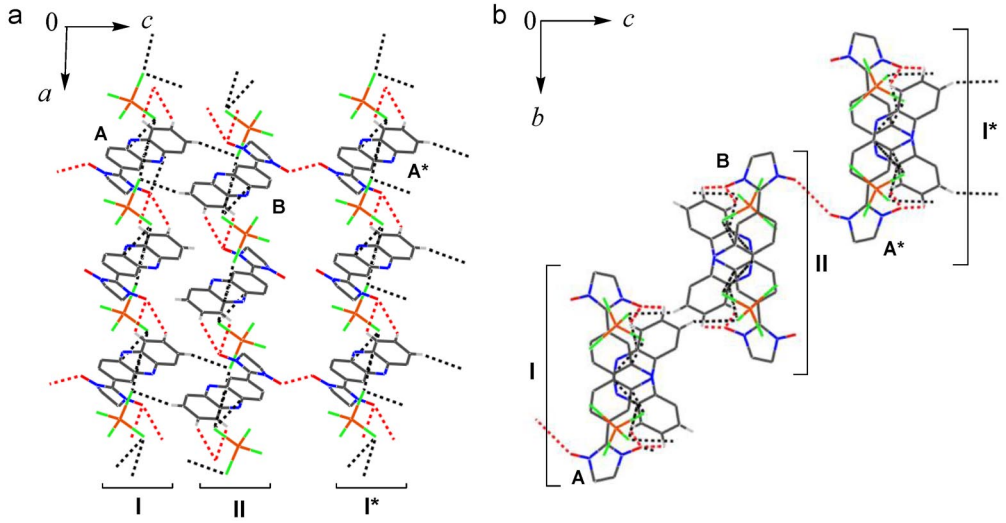

Fig. 1 Crystal packing structure of **NNDPP**$^{\bullet+}$·$FeCl_4^-$. (a) View projected along the *b*-axis. (b) View along the *a*-axis. The dotted lines show short contacts (black lines for the Cl–C and Cl–HC contacts, red lines for the O–HC and O–O contacts). The methyl and phenyl groups and most of hydrogen atoms are omitted for clarity.

Table 1 Crystallographic data for **NNDPP**$^{\bullet+}$·MX_4^- (M = Ga, Fe; X = Cl, Br).

	NNDPP$^{\bullet+}$·**$GaCl_4^-$**[a]	**NNDPP**$^{\bullet+}$·**$FeCl_4^-$**[b]	**NNDPP**$^{\bullet+}$·**$FeBr_4^-$**
formula	$C_{31}H_{29}Cl_4GaN_4O_2$	$C_{31}H_{29}Cl_4FeN_4O_2$	$C_{31}H_{29}Br_4FeN_4O_2$
fw	701.12	687.24	865.06
cryst syst	monoclinic	monoclinic	monoclinic
space group	$P2_1/a$ (#14)	$P2_1/a$ (#14)	$P2_1/a$ (#14)
a/Å	14.2533(7)	14.271(2)	13.8094(9)
b/Å	14.3424(6)	14.329(2)	15.6034(8)
c/Å	15.6136(7)	15.615(2)	15.0910(10)
β/degree	92.0050(19)	92.016(3)	100.736(4)
V/Å^3	3189.9(3)	3191.2(8)	3194.8(3)
Z value	4	4	4
T/K	123	123	93
F(000)	1432.00	1412.00	1700.00
μ/cm^{-3}	12.319 (Mo Kα)	8.413 (Mo Kα)	55.246 (Mo Kα)
reflns measured	22718	30837	23266
unique reflns	6916	7044	7023
observed reflns	6394 [$I > 2.00\sigma(I)$]	5246 [$I > 2.00\sigma(I)$]	20357 [$I > 2.00\sigma(I)$]
variables	408	408	408
refln/parameter	15.67	12.86	49.89
$R1$ [$I > 2.00\sigma$(I)]	0.0340	0.0475	0.0443
R_w	0.0484	0.0536	0.0670
GOF	1.088	0.886	1.006

[a]CCDC 749162.
[b]CCDC 749163.

The temperature dependence of χ_pT is shown in Fig. 2a. The χ_pT value at room temperature is 5.32 emu K mol^{-1}, which is close to the theoretical value (5.44 emu K mol^{-1} assuming g = 2.0157 from powder EPR) of the magnetically non-interacting **NNDPP**$^{\bullet+}$ (S = 1) and $FeCl_4^-$ (S = 5/2). The χ_pT value gradually decreases as the temperature is lowered, indicating antiferromagnetic interaction between **NNDPP**$^{\bullet+}$ and $FeCl_4^-$ (S = 5/2) and/or **NNDPP**$^{\bullet+}$s. This behavior is consistent with the crystal structure analysis.

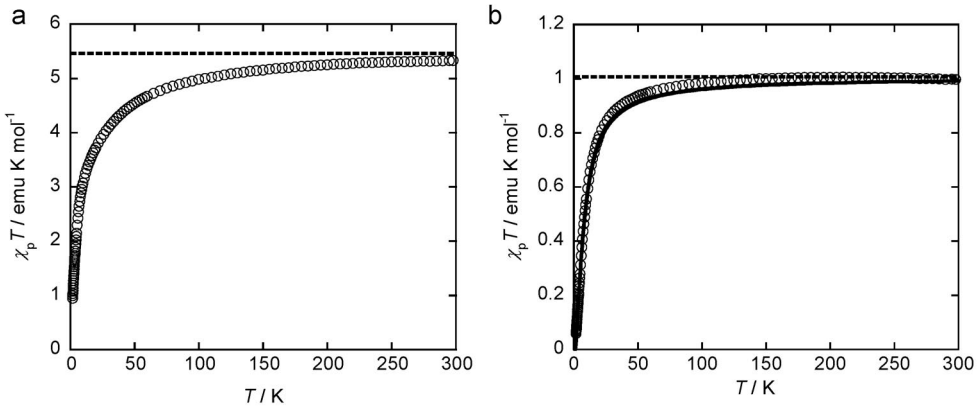

Fig. 2 The χ_pT-T plots for (a) **NNDPP**$^{\bullet+}$·$FeCl_4^-$ and (b) **NNDPP**$^{\bullet+}$·$GaCl_4^-$ under a magnetic field of 500 and 5000 Oe, respectively. The solid line in (b) is a simulation curve based on the dimer model ($\boldsymbol{H} = -2J\boldsymbol{S}_{S=1}\cdot\boldsymbol{S}_{S=1}$) with g = 2.0071 (powder EPR for **NNDPP**$^{\bullet+}$·$GaCl_4^-$) and J/k_B = –3.4 K.

The diamagnetic $GaCl_4^-$ salt is well known to have a quite similar molecular packing structure to the $FeCl_4^-$ salt [10]. We also studied the crystal structure and magnetic interaction of **NNDPP**$^{\bullet+}$·$GaCl_4^-$ to extract only the antiferromagnetic interaction between the organic moieties **NNDPP**$^{\bullet+}$s. The crystal of $GaCl_4^-$ salt belongs to the same space group ($P2_1/a$) and has very similar crystallographic parameters (Table 1). The molecular structure and molecular packing structure are very similar; the intermolecular short contacts are at Cl–C (3.27–3.46 Å), Cl–HC (2.81 Å), O–HC (2.61 and 2.68 Å), and O–O (3.02 Å) with a dihedral angle of 8.1° between the N–C=N plane and the benzo ring attached to the **NN**$^{\bullet}$ group. The χ_pT-T plots of the $GaCl_4^-$ salt are shown in Fig. 2b. The χ_pT value at room temperature is 1.0 emu K mol^{-1}, in accordance with the $S = 1$ (assuming $g = 2.0071$ from powder EPR) state at room temperature. The temperature dependence was simulated by the dimer model ($H = -2J\boldsymbol{S}_{S=1}\cdot\boldsymbol{S}_{S=1}$ solid line in Fig. 2b). The antiferromagnetic interaction due to the O–O contact is estimated to be $J = -3.4$ K. By comparing the $\chi_pT(T)$ curves between $GaCl_4^-$ and $FeCl_4^-$ salts, we note that the χ_pT value for the $FeCl_4^-$ salt starts to decrease at a higher temperature region (ca. <150 K) by lowering temperatures. This implies that the antiferromagnetic interaction in the $FeCl_4^-$ salts can be ascribed to both O–O contacts and Cl–C contacts.

NNDPP$^{\bullet+}$·$FeBr_4^-$ MAGNETIC PHASE TRANSITION INTO FERRIMAGNET

In contrast to **NNDPP**$^{\bullet+}$·$FeCl_4^-$, **NNDPP**$^{\bullet+}$·$FeBr_4^-$ exhibits phase transition into a ferrimagnet at T_c = 6.7 K [7a]. **NNDPP**$^{\bullet+}$·$FeBr_4^-$ has an identical space group with the $FeCl_4^-$ salt. The structure of **NNDPP**$^{\bullet+}$ moiety is very similar to the $FeCl_4^-$ salt; the dihedral angle between the N–C=N plane and the benzo ring attached to the **NN**$^{\bullet}$ group is 4.7°. They have different lattice parameters but a similar lattice volume (Table 1). The crystal packing structure of **NNDPP**$^{\bullet+}$·$FeBr_4^-$ is shown in Fig. 3. Several short contacts are also observed in this case (the Br atoms in $FeBr_4^-$, C atoms in **DPP**$^{\bullet+}$, and O atoms in **NN**$^{\bullet}$) at the Br–C contacts (3.50–3.70 Å) and the O–HC contacts (2.57 Å for a single contact, 2.53 Å for a double contact). Two types of columns, I and II, (–**NNDPP**$^{\bullet+}$–$FeBr_4^-$–**NNDPP**$^{\bullet+}$–$FeBr_4^-$–)$_n$s, are similarly formed along the *a*-axis through mainly the C–Br contacts. The O–HC contacts also combine

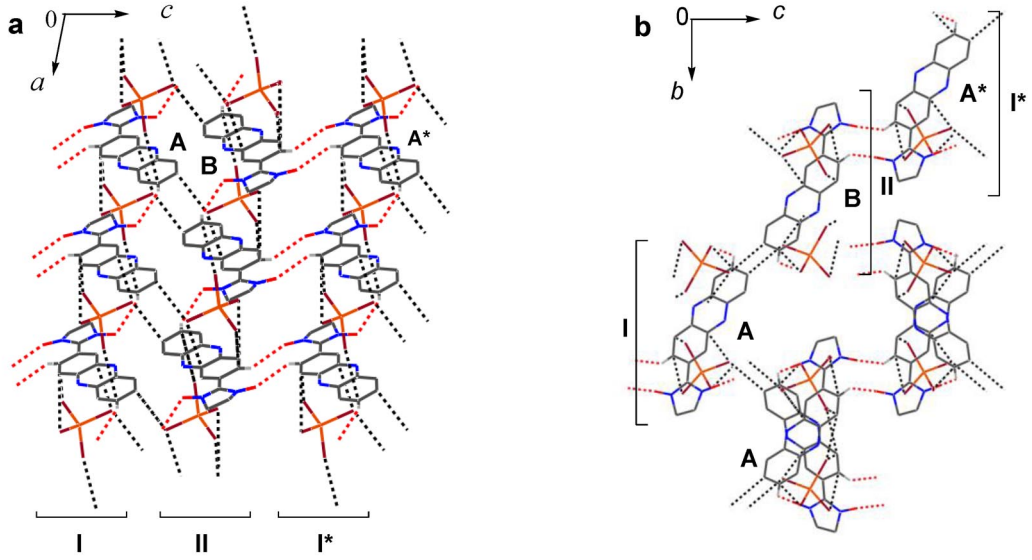

Fig. 3 Crystal packing structure of **NNDPP**$^{\bullet+}$·$FeBr_4^-$. (a) View projected along the *b*-axis. (b) View along the *a*-axis. The dotted lines show short contacts (black lines for the Br–C contacts, red lines for the O–HC contacts). The methyl and phenyl groups and most of hydrogen atoms are omitted for clarity.

NNDPP$^{\bullet+}$s within both columns I and II to make linear chains of **NNDPP**$^{\bullet+}$s along the *a*-axis. **NNDPP**$^{\bullet+}$ (**A**) in column I and the **NNDPP**$^{\bullet+}$ (**B**) in columns II are also bound by the C–Br contacts. Importantly, **NNDPP**$^{\bullet+}$ (**B**) in column II and **NNDPP**$^{\bullet+}$ (**A***) in column I* are bound by the double O–HC contacts in the $FeBr_4^-$ salts, which is in contrast to the single O–O contact between columns II and I* in the $FeCl_4^-$ salt (Fig. 1). The O–O distance in **NNDPP**$^{\bullet+}$·$FeBr_4^-$ is 3.78 Å, which is considerably longer than the sum (3.04 Å) of the van der Waals radii of the oxygen atoms. Thus, the column structures along the *a*-axis are combined by the C–Br contacts and the double O–HC contacts to form 2D network in the *a*–*c* plane. Furthermore, a similar combination of the Br–C and the double O–HC contacts is also observed along the *b*-direction. Thus, a 3D-type spin alignment is expected for **NNDPP**$^{\bullet+}$·$FeBr_4^-$.

On the basis of a theoretical study of the model compounds [7a], it is inferred that the Br–C contacts induce an antiferromagnetic interaction between the π-radical cation and the Fe(III) spins [11], whereas both O–HC contacts within columns and between columns II and I* induce ferromagnetic interaction between adjacent **NNDPP**$^{\bullet+}$ moieties. In columns I and II, the Br–C contact and O–HC contacts cooperatively function to give ferrimagnetic spin alignment between **NNDPP**$^{\bullet+}$ (S = 1) and $FeBr_4^-$ (S = 5/2). Further, these contacts along the *c* and *b* directions would induce ferromagnetic interactions between the **NNDPP**$^{\bullet+}$ (S = 1) spins.

The χ_pT-T plots (log scale in *x*-axis) are shown in Fig. 4a. The χ_pT value at room temperature is 5.61 emu K mol^{-1}, which is close to the theoretical value (5.59 emu K mol^{-1} using g = 2.008 for **NNDPP**$^{\bullet+}$ and g = 2.046 for $FeBr_4^-$ from powder EPR) for S = 5/2 (Fe(III)) plus S = 1 (**NNDPP**$^{\bullet+}$). As the temperature is lowered, χ_pT gradually decreases to the minimum value (3.93 emu K mol^{-1} at 18 K) and sharply increases below 18 K. Such temperature dependence is typical for a ferrimagnetic spin alignment. Further, χ_pT reaches the maximum value (39.7 emu K mol^{-1}) around 6 K and sharply drops at lower temperatures (<6 K). To obtain an insight into the sharp drop below 6 K, experiments were performed under field-cooled (FC) and zero-field-cooled (ZFC) conditions. The M(T) curves sharply split at 7.0 K, and the remnant magnetization (M_R) disappeared in the same temperature region (Fig. 4a, inset). These results suggest the onset of a phase transition into a ferrimagnetic ordered state (T_c = 6.7 K) [7a].

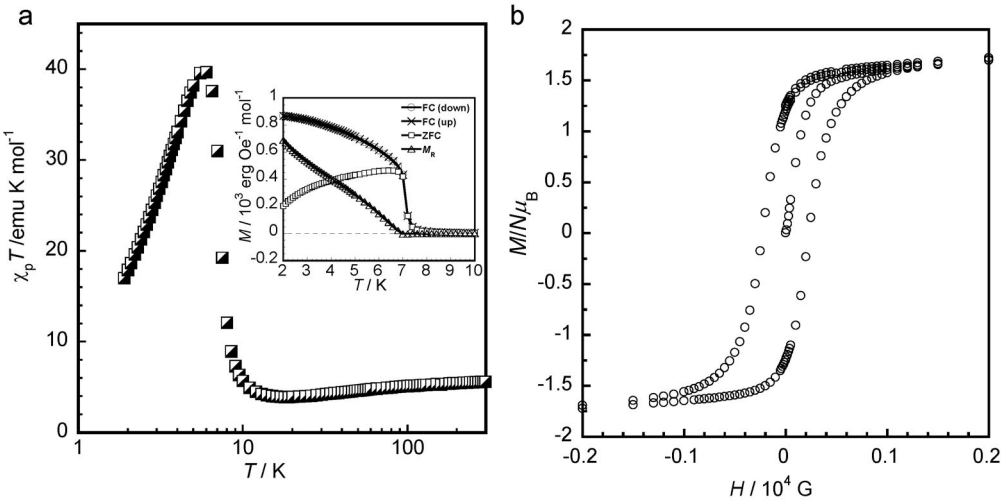

Fig. 4 Magnetic properties of **NNDPP**$^{\bullet+}$·$FeBr_4^-$. (a) χ_pT-T plots under a magnetic field of 1000 Oe; the temperature axis is plotted on a log scale for expansion of the low-temperature region. (b) M-H curve at 1.9 K; M_R = 1.2 $N\mu_B$ and H_C = 230 Oe.

Figure 4b presents a magnetic hysteresis curve at 1.9 K, that shows a remnant magnetization of M_R = 1.2 $N\mu_B$ and a coercive field of H_C = 230 Oe. The magnetization curve $M(H)$ saturates under a higher field of ~7 T. The saturation magnetization value (M_S = 3.08 $N\mu_B$) is in good agreement with the theoretical value ($M_S = g\mu_B\Delta S$ = 3.05 $N\mu_B$) at ΔS = (5/2 – 1), indicating a phase transition into a ferrimagnet. The smaller M_R value compared to the M_S value is due to the magnetocrystalline anisotropy, which is frequently observed in ferrimagnetic molecular systems [12].

The temperature dependence of heat capacities for **NNDPP**$^{\bullet\bullet+}$·$FeBr_4^-$ was also measured. The phase-transition temperature was determined from the sharp peak of the magnetic heat capacities (T). The magnetic entropy at the zero magnetic field was evaluated to be 23.8 J K^{-1} mol^{-1}. This value agrees well with the expected value for a spin system composed of S = 1 (**NNDPP**$^{\bullet\bullet+}$) and S = 5/2 (Fe(III)), $R\ln(3 \times 6)$ = 24.0 J K^{-1} mol^{-1} [7a].

CONCLUSION

Stable radical-substituted radical cations (**NNDPP**$^{\bullet\bullet+}$s) based on the dihydrophenazine structure were prepared. **NNDPP**$^{\bullet\bullet+}$s have a large and positive intramolecular exchange interaction between **NN**$^{\bullet}$ and **DPP**$^{\bullet+}$. Introducing the third spin as a counter anion produces a unique three-spin system. The structures and magnetic properties of **NNDPP**$^{\bullet\bullet+}$·$FeCl_4^-$ and **NNDPP**$^{\bullet\bullet+}$·$FeBr_4^-$ salts were compared: **NNDPP**$^{\bullet\bullet+}$·$FeCl_4^-$ showed antiferromagnetic interaction at low temperature (<150 K), whereas **NNDPP**$^{\bullet\bullet+}$·$FeBr_4^-$ underwent magnetic phase transition at T_c = 6.7 K into a ferrimagnet. These two salts have similar molecular structures. Intermolecular short contacts were analyzed in detail. The most striking difference in these salts was found to be in arrangement of the nearest neighboring **NNDPP**$^{\bullet\bullet+}$s; specifically, the antiferromagnetic O–O contact was observed in **NNDPP**$^{\bullet\bullet+}$·$FeCl_4^-$, whereas the ferromagnetic double O–HC contacts were observed in **NNDPP**$^{\bullet\bullet+}$·$FeBr_4^-$.

Because of subtle differences in the sizes and positions of the $FeCl_4^-$ and $FeBr_4^-$ anions, the relative orientation of **NNDPP**$^{\bullet\bullet+}$s changes. The overall change in packing structure should be reflected in the lattice parameters. The differences in the unit cell lengths a and c are small (<3.5 %). However, for the $FeBr_4^-$ salt, the unit cell length b and angle β are longer and larger, respectively, by ~10 %. Such a deformation would facilitate the ferromagnetic O–HC contact.

REFERENCES

1. K. Yamaguchi, H. Namimoto, T. Fueno. *Chem. Phys. Lett*. **166**, 408 (1990).
2. (a) T. Sugano, T. Fukasawa, M. Kinoshita. *Synth. Met*. **43**, 3281 (1991); (b) H. Sakurai, A. Izuoka, T. Sugawara. *J. Am. Chem. Soc*. **122**, 9723 (2000).
3. Y. Nakamura, N. Koga, H. Iwamura. *Chem. Lett*. 69 (1991).
4. (a) J. Nakazaki, Y. Ishikawa, A. Izuoka, T. Sugawara, Y. Kawada. *Chem. Phys. Lett*. **319**, 385 (2000); (b) R. Kumai, M. M. Matsushita, A. Izuoka, T. Sugawara. *J. Am. Chem. Soc*. **116**, 4523 (1994).
5. (a) T. Sugimoto, S. Yamaga, M. Nakai, K. Ohmori, M. Tsuji, H. Nakatsuji, H. Fujita, J. Yamauchi. *Chem. Lett*. 1361 (1993); (b) T. Sugimoto, S. Yamaga, M. Nakai, M. Tsuji, H. Nakatsuji, N. Hosoito. *Chem. Lett*. 1817 (1993).
6. P. L. Nordio, Z. G. Soos, H. M. McConnell. *Ann. Rev. Phys. Chem*. **17**, 237 (1966).
7. (a) Y. Masuda, M. Kuratsu, S. Suzuki, M. Kozaki, D. Shiomi, K. Sato, T. Takui, Y. Hosokoshi, X.-Z. Lan, Y. Miyazaki, A. Inaba, K. Okada. *J. Am. Chem. Soc.* **131**, 4670 (2009); (b) S. Hiraoka, T. Okamoto, M. Kozaki, D. Shiomi, K. Sato, T. Takui, K. Okada. *J. Am. Chem. Soc*. **126**, 58 (2004).
8. (a) M. M. Matsushita, H. Kawakami, T. Sugawara, M. Ogata. *Phys. Rev. B* **77**, 195208 (2008); (b) M. M. Matsushita, H. Kawakami, Y. Kawada, T. Sugawara. *Chem. Lett*. **36**, 110 (2007).

9. Y. Masuda, M. Kuratsu, S. Suzuki, M. Kozaki, D. Shiomi, K. Sato, T. Takui, K. Okada. *Polyhedron* **28**, 1950 (2009).
10. M. Kuratsu, S. Suzuki, M. Kozaki, D. Shiomi, K. Sato, T. Takui, K. Okada. *Inorg. Chem*. **46**, 10153 (2007).
11. A. Miyazaki, M. Enomoto, M. Enomoto, T. Enoki, G. Saito. *Mol*. *Cryst. Liq. Cryst*. **305**, 425 (1997).
12. (a) K. Inoue, T. Hayamizu, H. Iwamura, D. Hashizume, Y. Ohashi. *J. Am. Chem. Soc*. **118**, 1803 (1996); (b) O. Kahn, Y. Pei, M. Verdaguer, J. P. Renard, J. Sletten. *J. Am. Chem. Soc*. **110**, 782 (1988).

